J. Cent. South Univ. (2015) 22: 2540−2548
DOI: 10.1007/s11771-015-2783-4

Springer

Multi-objective optimization of crimping of large-diameter welding pipe

FAN Li-feng(范利锋)[1], GAO Ying(高颖)[2], YUN Jian-bin(云建斌)[3], LI Zhi-peng(李志鹏)[4]

1. Transportation Institute, Inner Mongolia University, Hohhot 010070, China;
2. College of Material Science and Engineering,
Hebei University of Science and Technology, Shijiazhuang 050018, China;
3. Product Quality Inspection Institute of Inner Mongolia, Hohhot 010070, China;
4. Institute of Aircraft Design, Shenyang 110035, China

Abstract: Crimping is widely adopted in the production of large-diameter submerged-arc welding pipes. Traditionally, designers obtain the technical parameters for crimping from experience or by trial and error through experiments and the finite element (FE) method. However, it is difficult to achieve ideal crimping quality by these approaches. To resolve this issue, crimping parameter design was investigated by multi-objective optimization. Crimping was simulated using the FE code ABAQUS and the FE model was validated experimentally. A welding pipe made of X80 high-strength pipeline steel was considered as a target object and the optimization problem for its crimping was formulated as a mathematical model and crimping was optimized. A response surface method based on the radial basis function was used to construct a surrogate model; the genetic algorithm NSGA-II was adopted to search for Pareto solutions; grey relational analysis was used to determine the most satisfactory solution from the Pareto solutions. The obtained optimal design of parameters shows good agreement with the initial design and remarkably improves the crimping quality. Thus, the results provide an effective approach for improving crimping quality and reducing design times.

Key words: crimping; welding pipe; optimization; grey system theory; genetic algorithm

1 Introduction

Crimping technology is widely used in the manufacture of large-diameter straight-seam submerged arc welded (LSAW) pipes. In the crimping process, both edges of a sheet are bent into a certain curvature using a crimping die. Then, the edges of the sheet are made to approach to or completely attain the nominal curvature of the pipe. The geometry and dimensional accuracy of final products are obtained. The crimping process effectively prevents the peach beak and cracking during expansion.

Factors affecting crimping quality can be divided into two categories for a certain sheet material: (1) factors related to the mould, such as tooling geometry and mould set-up parameters, and (2) factors related to the bending process, such as the forming force. Several studies have been conducted on these parameters and their effects on crimping quality. In general, crimping is investigated by three research approaches: research based on experience, research based on analytical methods, and research by finite element analysis.

In early stages of research on crimping, the approach was to conduct studies based on production experience. For example, LI [1] clarified the crimping process and its technical parameters. XIE and XIA [2] summarized optimum ranges of parameters of crimping on the basis of long-term production experience. However, though the results of such experience-based studies are useful as guides during production, they lack universality and practical applicability.

The research approach of using analytical methods is based on simplifications of the crimping process and behaviour of the material used. In an early attempt, XIE and XIA [2] obtained a few theoretical results for crimping by adopting material mechanics, which was based on the hypothesis that the materials undergo pure plastic deformation and no hardening. ZHAO [3] developed a formula for the bending moment and forming force for a bilinear elasto-plastic hardening material model. YANG [4] derived calculation formulas for springback in crimping using a power exponential hardening material model and a bilinear hardening

Foundation item: Project(Y2012035) supported by the Natural Science Foundation of Hebei Provincial Education Department, China; Project(12211014) supported by the Natural Science Foundation of Hebei Provincial Technology Department, China; Project(NJZY14006) supported by the Inner Mongolia Higher School Science and Technology Research Program, China; Project(2014BS0502) supported by the Natural Science Foundation of Inner Mongolia, China; Project(135143) supported by the Program of Higher-level Talents Fund of Inner Mongolia University, China
Received date: 2014−06−24; **Accepted date:** 2014−09−15
Corresponding author: FAN Li-feng, PhD; Tel: +86−471−4996252; E-mail: ysufanlifeng@foxmail.com

material model. FAN et al [5] obtained a more accurate analytical solution for springback and the forming force based on the Hill theory of precise bending. However, the drawback of using analytical methods is that they require significant simplifications of the forming conditions, which in turn can considerably hamper the result accuracy.

The advent of computational technologies has resulted in the use of the finite element method (FEM) to analyse the simulation of crimping. Then, several research groups have analysed the effect of crimping on the pipe quality using the FEM. For example, PALUMBO and TRICARICO [6] analysed the crimping process using the FEM and obtained the stress and strain in the cross-section of a sheet. LIU et al [7] studied the effect of crimping on the forming of the O-shape in U-shape-O-shape-expanding (UOE) forming. HERYNK et al [8] analysed the effect of crimping on the pipe failure pressure. Further, TONG [9] researched the effect of crimping on welding grooves and striking angles of the welding on the sheet. GAO et al [10] analysed crimping using the finite element software ABAQUS under the assumption of moulds being simplified to arcs and obtained the relationship between the die displacement and the bending angle and corresponding equation of this relationship using regression analysis. REN et al [11] obtained the maximum forming force using a three-dimensional FE model. Despite finite element analysis (FEA) being an efficient tool for investigating the crimping process, the large amount of time required to design crimping parameters is the most significant disadvantage of FEA.

With the requirement of crimping quality becoming increasingly stringent, the design of crimping parameters has become a major concern in manufacturing LSAW pipes. The conventional design process is largely based on a trial-and-error approach. As a result, obtaining the ideal crimping parameters for a new welding pipe often requires numerous trials, leading to a long design cycle and significantly high cost. However, this problem can be solved using computational optimization. To this end, OHATA et al [12] adopted the sweeping simplex method with FEA to optimize the punch travel and forming stages for obtaining a uniform thickness distribution. NACEUR et al [13] employed a mathematical programming algorithm in an inverse procedure to first optimize the restraining forces and then design the draw bead. AZAOUZI et al [14] developed an automatic design procedure in a commercial FEA program and adopted a heuristic optimization algorithm (HOA) for the blank shape design of high-precision metallic parts in a special stamping process. GUO et al [15] combined an inverse procedure with a sequential quadratic programming (SQP) technique to optimize the blank shape. Therefore, computational optimization represents a more effective tool in that it seeks ideal crimping parameters systematically, which in turn helps engineers to achieve the optimum crimping quality.

The aim of this work is to show that optimization of crimping using computational methods such as the response surface model (RSM), genetic algorithm (GA), and grey relational analysis (GRA) is an effective approach to achieve optimum crimping quality. The basis of this approach is the forming analysis performed using experiments and the commercial FEA code ABAQUS. Through crimping optimization, the ideal crimping parameters, i.e. the base radius of the punch, R_p, the terminal angle of the punch, β_p, the length of a crimp, B, and forming force, F, are obtained.

2 Analysis of crimping process

2.1 Experiment

2.1.1 Crimping process

In this process, the crimping punch and sheet were fixed. First, the sheet was clamped by two holders and the crimping die was raised gradually. Then, the sheet edge was bent gradually starting from point O along the shape of the punch. With the progress of sheet forming, the curvature of the sheet edge increased and the force arm shortened. The sheet began unloading and springback occurred when the die achieved the setting displacement. Later, crimping was completed, as shown in Fig. 1. It included forming moulds and their geometry relationship.

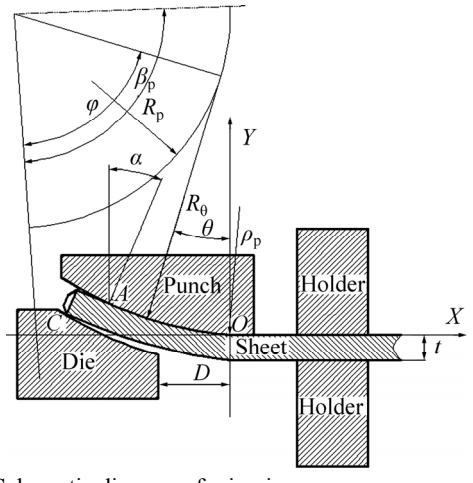

Fig. 1 Schematic diagram of crimping process

An involute was adopted to design the shape of the crimping punch and die. The parameter equation of the involute can be expressed in the Cartesian coordinate system as follows:

$$\begin{cases} x(\phi) = R_p \cos\phi + \phi R_p \sin\phi \\ y(\phi) = R_p \sin\phi - \phi R_p \cos\phi \end{cases} \quad (1)$$

where R_p is the base radius and φ is the base angle.

A new XOY coordinate system, where O is the original point that is the involute end point corresponding to the terminal angle β_p, is built.

The parameter equation of the punch is expressed in the XOY coordinate system as follows:

$$\begin{cases} X(\phi)=[x(\phi)-x(\beta_p)]\cos\beta_p+[y(\phi)-y(\beta_p)]\sin\beta_p \\ Y(\phi)=-[x(\phi)-x(\beta_p)]\sin\beta_p+[y(\phi)-y(\beta_p)]\cos\beta_p \end{cases} \quad (2)$$

The relationship among the involute angle φ, crimping bending angle θ, and curvature radius R_θ of the punch can be written as follows:

$$\begin{cases} \theta=\beta_p-\phi \\ R_\theta=R_p\cdot\phi \end{cases} \quad (3)$$

The straight edge length L_Z in Eq. (4) can be expressed as

$$L_Z=B-\left(R_p\alpha\beta_p-\frac{R_p}{2}\alpha^2\right)-\frac{t}{2}\tan\alpha-P \quad (4)$$

The central angle α' of the pipe is related to the crimp length as

$$\alpha'=\frac{B}{R_n-t/2} \quad (5)$$

where R_n is the nominal outer radius of the pipe.

The central angle α'' of the pipe is related to the straight edge L_Z as

$$\alpha''=\arctan\left(\frac{L_Z}{R_n-t/2}\right) \quad (6)$$

And the target bending angle α_t after springback is given as

$$\alpha_t=\alpha'-\alpha'' \quad (7)$$

There is a condition that the crimping bending angle after springback α_y must be equal to a target bending angle in crimping process. To weigh the curvature radius of crimping after springback, the equivalent radius of curvature, R', is defined as

$$R'=\frac{B-L_Z-P}{\alpha_y} \quad (8)$$

Therefore, the greater the approximation of the equivalent radius of curvature to the nominal radius of curvature is, the better the crimping quality is.

2.1.2 Experimental material and equipment

The sheet metal used in crimping experiments was Q235A, with its basic mechanical properties listed in Table 1. Here, E and σ_s denote the elastic modulus and tensile yield stress, respectively, of the metal. n is the power-law strain hardening exponent and K is the strength coefficient.

The crimping moulds used in the experiment were shrunk to one-third the size of the actual production mould, and their geometric parameters are listed in Table 2.

Table 1 Material properties of sheet metal used in experiments

E/GPa	v	n	K/MPa	σ_s/MPa
210	0.3	0.245	490	363

Table 2 Geometric parameters of crimping in experiment

Parameter	Value
Base radius of punch, R_p/mm	101.6
Terminal angle of punch, β_p/(°)	88
Crimp length, B/mm	63.3

The experiments were performed in a 3150 kN hydraulic press, which is normally used for the try-outs of production tools. The press was equipped with sensors for measuring the punch force. All sensors were connected to a PC system. Figure 2 shows a picture of the tool in the press in the crimping experiment. The bending angle before and after springback was measured using a portable three-coordinate measuring system. The estimated measurement error was 0.02 mm.

2.1.3 Experimental procedure.

In this work, over 20 experiments were performed on the Q235A in order to validate the FE model. The forming process can be seen in crimping experiments. The forming force could be adjusted by controlling the die displacement. The crimping parts are shown in Fig. 3.

The crimping experiments were performed in the following steps.

1) The sheet is fixed between the holders.

2) The die is moved up to a pre-set displacement point that satisfies the assumed forming force.

3) The bending angle before springback is measured using the measuring system.

4) The die moves back down.

5) The bending angle after springback is measured using the measuring system.

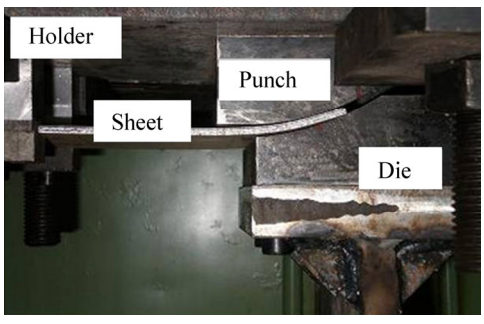

Fig. 2 Photograph of crimping experiment

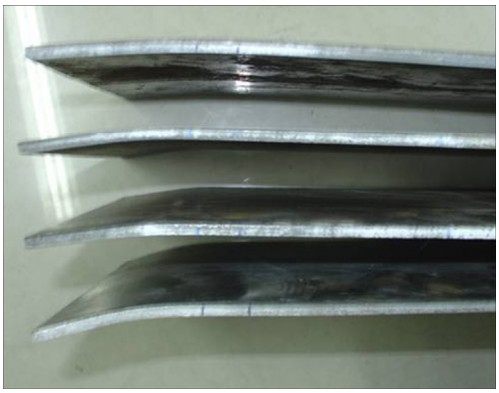

Fig. 3 Crimping parts in experiment (Comparison of crimping parts with different die displacement: h_1=8.32 mm, h_2=9.318 mm, h_3=10.03 mm and h_4=13.95 mm)

2.2 FEA

FEA was performed using the commercial code ABAQUS/Standard. Because of wide bending angles of the sheet metal, a two-dimensional FE model was established for the plane strain condition. The set-up of this model is shown in Fig. 4. In the FE model, the discrete rigid body is defined in punch and die. The 2 mm CPE4R is set in the deformable sheet.

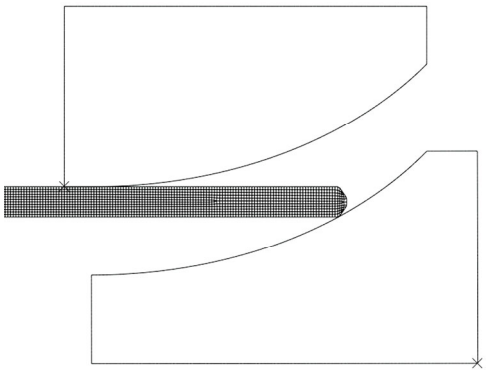

Fig. 4 Set-up of FE model

Crimping equipment is usually composed of the die, punch, holder and sheet. In our FE model, the holder is defined as analytical rigid body which would not need elements for simple geometric shapes. The discrete rigid body and 2.5 mm R2D2 element are defined in punch and die without considering the deformation. Considering the both efficiency and the accuracy of the deformation process, the 2 mm four-node, plane-strain, reduced integration quadrilateral element CPE4R which has high efficiency and accuracy for calculating springback is set in the deformable sheet. The sheet metal is defined to be elastoplastic.

The FE model convergence is amended by reducing the minimum iteration and improving the contact-state stability. Further, a simple, limited slide master−slave contact algorithm in which the mould is the master surface and the sheet is the slave surface is employed, and the penalty function model with a friction coefficient of 0.1 is used to determine the contact state. This model enables the elastic slide and the sheet surface to be invaded by the mould, which does not increase the degrees of freedom of the system but greatly improves the computational efficiency.

The objectives of this FEA are to investigate the forming law and also the relationship between influential crimping factors and forming quality. Furthermore, the data obtained in this analysis are intended to be used as training data for a surrogate model.

3 Multi-objective optimization process

In the optimal design of crimping, multi-objectives must be considered under the given constraint. The GA, which has large-scale randomness and parallel search features, is presently a popular method for solving the multi-objective optimization problem. However, our optimization process is faced with the following two problems.

1) Optimization is usually an iterative process. An optimal design requires hundreds of finite element analyses to converge, and each forming simulation often incurs considerable computational cost. Therefore, the practical applicability of optimization using GA will be largely compromised. For this purpose, a surrogate model based on the RSM is considered as a more effective approach.

2) Generally, an optimal solution set (Pareto solution set) exists in multi-objective optimization. However, the most reasonable and ideal result in the context of an engineering project is rarely selected from Pareto optimal results. Therefore, in this work, GRA was used to analyse the uncertainty associated with determining the ideal result.

Then, the flowchart of the optimization process is shown in Fig. 5.

In this work, the design variables, constraint conditions, and optimized objectives were determined by analysing the multi-objective optimization problem. Then, crimping was simulated using ABAQUS and the reliability of the FE model was verified experimentally. A surrogate model based on the radial basis function (RBF) was constructed by inputting data points from design simulation schemes. The Pareto optimal solution set was found using the fast non-dominated sorting GA (version II), i.e. NSGA-II, and the optimal design scheme was determined using GRA.

3.1 Problem description

The problem of crimping optimization was to determine the set of crimping parameters $\boldsymbol{x}^{\mathrm{T}}=(x^1, x^2, x^3, x^4)$, i.e. the base radius of the punch, R_{p}, the terminal

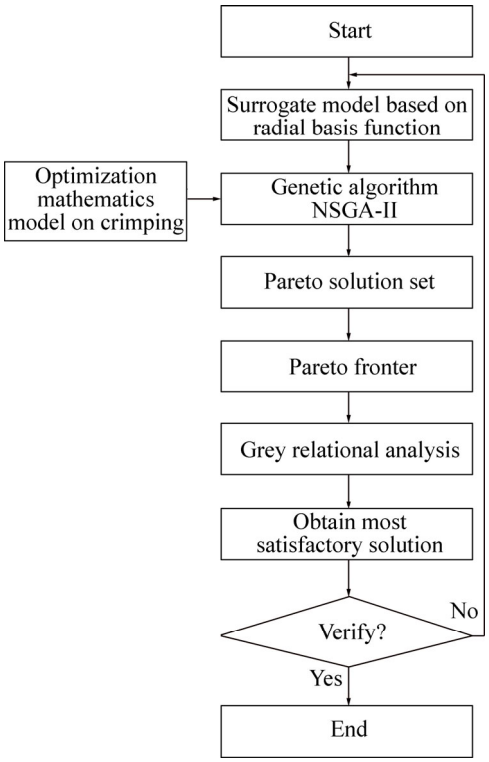

Fig. 5 Flowchart of crimping optimization

angle of the punch, β_p, the crimp length, B, and the forming force F_y that minimizes the straight edge L_Z and the absolute value of the differences between the nominal radius of curvature and the equivalent radius of curvature. The optimization problem can be stated as

$$\min\begin{cases} f_1(x)=L_Z \\ f_2(x)=\left|R'-R_n\right| \end{cases} \tag{9}$$

At the same time, according to Section 2.1.1 and crimping quality standards in production, the constraint conditions were set up as follows:

$$\text{s.t.}\begin{cases} g_1(x)=\left|\alpha_y-\alpha_t\right|-\varepsilon_1\le 0 \\ g_2(x)=L_Z-1.5t\le 0 \\ g_3(x)=\left|R'-R_n\right|-\varepsilon_2\le 0 \end{cases} \tag{10}$$

$$\boldsymbol{x}^{\mathrm{T}}=(x_1,x_2,x_3,x_4)=(R_p,\beta_p,F_y,B) \tag{11}$$

In this work, ε_1=0.1, ε_2=30 and t=22.

$$\begin{cases} 240\ \text{mm}\le x_1\le 340\ \text{mm} \\ 68\ \text{mm}\le x_2\le 108\ \text{mm} \\ 0\ \text{kN}\le x_3\le 4000\ \text{kN} \\ 150\ \text{mm}\le x_4\le 230\ \text{mm} \end{cases} \tag{12}$$

3.2 Surrogate model

An RSM-based RBF is widely used as the surrogate model of an actual problem in several fields. RBF is a function whose variables are Euclidean distances between sample points and calculation points. Its basic form can be expressed as follows:

$$f(\boldsymbol{x})=\sum_{i=1}^{m}\beta_i\varphi(r_i,c) \tag{13}$$

$$\boldsymbol{\beta}=\begin{bmatrix}\beta_i\\ \vdots\\ \beta_m\end{bmatrix},\ \boldsymbol{\varphi}=\begin{bmatrix}\varphi(r_1,c)\\ \vdots\\ \varphi(r_i,c)\end{bmatrix}$$

Here, $r_i(\boldsymbol{x})=\|x-x_i\|$, i.e. Euclidean distances between $\boldsymbol{x}_i$ and x; c is a nonnegative constant; β is a weighting coefficient.

The base function can be expressed in Gaussian form as

$$\varphi(r_i,c)=\exp(-r^2/c^2) \tag{14}$$

The following interpolation condition must be satisfied:

$$f(x_i)=F(x_i) \tag{15}$$

The following equation is obtained:

$$\boldsymbol{A}\cdot\boldsymbol{\beta}=\boldsymbol{F} \tag{16}$$

$$\boldsymbol{A}=\begin{bmatrix}\varphi(x_1-x_1) & \cdots & \varphi(x_1-x_m)\\ \vdots & \vdots & \vdots\\ \varphi(x_m-x_1) & \cdots & \varphi(x_m-x_m)\end{bmatrix},\ \boldsymbol{F}=\begin{bmatrix}F(x_1)\\ \vdots\\ F(x_m)\end{bmatrix}$$

When $\varphi(r_i, c)$ is a positive definite function, there is only one solution:

$$\boldsymbol{\beta}=\boldsymbol{A}^{-1}\cdot\boldsymbol{F} \tag{17}$$

Finally, the response surfaces are generated in the following steps:

1) Determine the design variables (factors) and crimping quality (responses).

2) Arrange the factors sampled with the design of experiment methodology in an array.

3) Perform numerical experiments using FEA and extract the response values from the simulation results.

4) Construct the surrogate model using RSM-based RBF.

5) Evaluate the errors of the surrogate model.

3.3 NSGA-II

NSGA-II was used for optimization. It is a multi-objective evolutionary algorithm that uses the elite preservation strategy and an explicit diversity-preserving mechanism to find a set of evenly distributed solutions of a multi-objective optimization problem. NSGA-II was originally developed to reduce computational complexity, improve the diversity among non-dominated solutions, and add elitism to NSGA. The simplicity, effectiveness, and independence from user-defined parameters make NSGA-II a flexible and robust evolutionary algorithm for

solving various multi-objective optimization problems using a common framework. However, it needs a large number of function evaluations to find the Pareto optimal set. Therefore, in this work, a surrogate model was used to reduce the cost of the optimization process.

Further details on NSGA-II were found by YUSOFF et al [16]. In this work, the population size, generation count, and crossover and mutation probabilities were set in such a way that the best solutions would be obtained [17]. The population size was set to be 8 for the run where a random seed was used for the generation of the initial population. Convergence was achieved by the end of the 200th generation. Finally, the crossover probability and mutation probability were set to be 0.65 and 0.1, respectively. The Pareto optimal front was obtained using NSGA-II.

3.4 GRA

The engineering project was selected from Pareto optimal results according to experience of technical personnel, but the result was often limited by understanding of the problem and practical experience of the designer. So, it is difficult to determine the most satisfactory solution from the Pareto set. This difficulty was overcome by using GRA, which is commonly used in decision making. It is an impact evaluation model that measures the degree of similarity or difference between two sequences based on the relational grade.

A global comparison among the alternatives is generated using the GRA in the following four steps [18−20].

1) Normalize the results of the Pareto optimal front for all the trials.

2) Derive the reference sequences.

3) Calculate the grey relational coefficient.

4) Determine the grey relational grade.

The higher the grey relational grade is, the closer the result to the ideal normalized value is.

4 Results

4.1 Experimental results

The results of crimping experiments were compiled to validate the FE model and evaluate the effect of die displacement on springback. Figures 6 and 7 show the comparisons between the experimental results and FEA.

From these figures, the following observations are made:

1) The bending angle before or after springback increases with the increase in die displacement.

2) The forming force increases with the increase in die displacement.

3) The FEA shows errors of about 1.24° (Fig. 6) and 2.2 kN (Fig. 7). These errors are within an acceptable range, confirming that the FE model results are in good agreement with the experimental results.

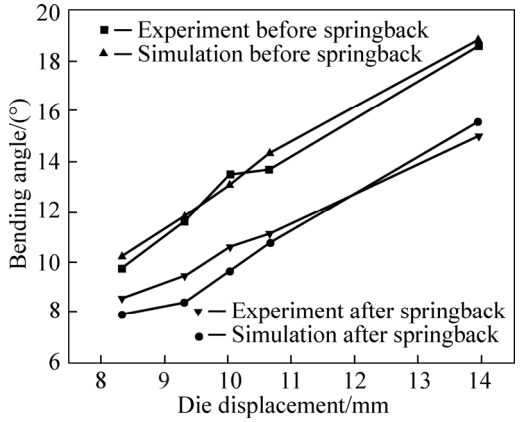

Fig. 6 Comparison of bending angle between results of experiment and FEA

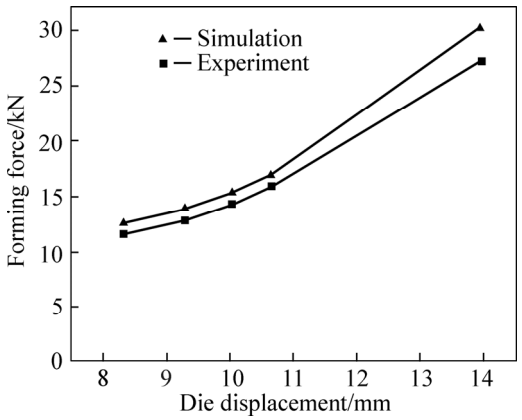

Fig. 7 Comparison of forming force between results of experiment and FEA

4.2 FEA results

A welding pipe of high-strength pipeline steel X80 with dimensions of *d*1219 mm×22 mm×12000 mm was taken as the research target. Figure 8 shows the actual stress–strain curve of X80, with E=245 GPa and σ_s= 569.5 MPa. Figure 9 shows the geometry and residual stress distribution of crimping after unloading. It is

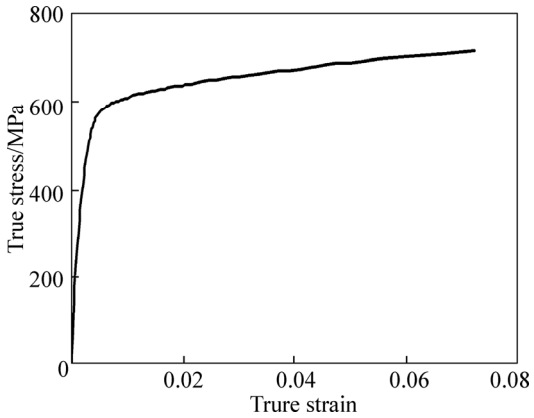

Fig. 8 Stress−strain curve of X80 steel

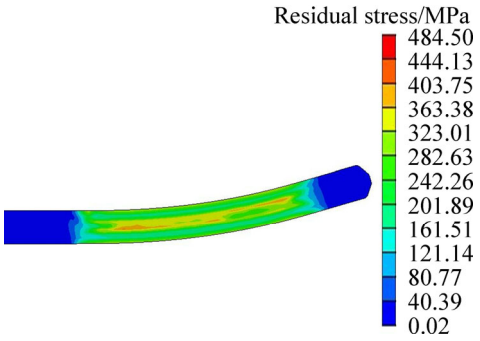

Fig. 9 Geometry and residual stress distribution of crimping after unloading obtained from FEA

known that there is no stress and no deformation near the edge of sheet.

The FEA results are used as training data for the surrogate model. The arrangement of simulation as training data is constituted by the optimal Latin hyper-cube sampling (OLHS) approach. As mentioned earlier, the main crimping parameters to be simulated include the base radius R_p of the punch, the terminal angle β_p of the punch, forming force F, and crimp length B. A total of 30 sample points were provided as inputs to the surrogate model, as listed in Table 3.

4.3 Optimization results

4.3.1 Results of surrogate model

Several common indicators were used to evaluate the RSM's validity in this work: the relative root mean squared error (RMSE), the average relative error (ARE), and the coefficient of determination, R^2. Their determined values for the RSM are listed in Table 4.

Table 3 Sampling according to optimal Latin hyper-cube (OLHS) from simulation results

Sample number	B/mm	F_y/kN	R_p/mm	β_p/(°)	α_y/(°)	L_Z/mm	R'/mm
1	188.689	1404.4	301.1079	88.6072	12.606	47.902	639.898
2	196.555	689.741	284.3713	70.4	8.940	90.487	679.775
3	201.799	2651.9	355.4717	97.0992	12.233	28.332	812.461
4	222.756	569.505	292.7396	75.2576	8.392	107.360	787.897
5	193.933	680.224	255.1125	84.964	7.899	93.299	730.002
6	225.378	3399.96	334.5509	87.3928	19.741	23.781	387.356
7	214.89	4515.2	267.665	100.7424	21.096	17.807	528.149
8	165.11	2062.93	330.397	72.8288	14.180	34.225	528.854
9	186.067	1663.8	317.8446	95.8936	11.036	42.023	747.804
10	154.622	1201.31	296.9238	86.1784	7.413	57.531	750.419
11	207.043	717.828	347.1034	71.6144	9.095	87.430	753.497
12	209.646	2198.74	326.2129	80.1064	19.481	31.909	476.530
13	172.957	1838.48	246.7442	94.6792	14.649	37.931	528.131
14	175.579	2954.02	280.1871	105.6	12.526	26.275	682.937
15	204.421	650.331	242.56	81.3208	9.253	94.849	483.643
16	220.134	3932.26	342.9192	98.3136	13.949	24.079	826.832
17	183.445	1568.99	351.2875	101.9568	12.663	44.170	725.085
18	167.732	1568.99	305.2921	77.6864	12.661	44.170	796.309
19	191.311	2361.74	338.735	78.9008	16.483	31.176	529.297
20	180.823	1115.17	271.8491	74.0432	14.333	58.349	437.260
21	162.488	780.289	359.6558	89.8216	2.766	86.912	2162.267
22	228	939.718	276.003	82.5352	18.381	63.793	470.978
23	199.177	1307.49	288.5554	91.036	13.742	50.022	468.932
24	170.354	752.552	313.6604	103.1712	3.241	90.080	2438.354
25	178.201	4844.48	363.84	83.7496	14.013	22.470	722.527
26	159.866	1394.67	263.4808	76.472	12.949	49.761	415.003
27	152	922.575	322.0287	93.4648	3.627	74.156	1643.383
28	217.512	2474.89	250.9283	99.528	21.554	29.806	505.943
29	157.244	3452.67	259.2966	92.2504	14.095	28.349	502.638
30	212.268	3826.27	309.4762	104.3856	15.284	24.172	764.103

Table 4 Indicators of validity of model for evaluating crimping quality

Crimping parameter	RMSE	ARE	R^2
Length of straight edge, L_Z/mm	0.02463	0.01778	0.9874
Equivalent radius of curvature, R'/mm	0.00549	0.00392	0.99907
Maximum horizontal forming force F_x/kN	0.02137	0.01388	0.98789
Maximum vertical forming force F_y/kN	0.01005	0.0087	0.9925

The closer the value of R^2 to 1 is, the better the fit of the model is (R^2 ranges from 0 to 1). It is important to make basis for the optimal design, and hundreds of calculations can be completed in short time.

4.3.2 Results of NSGA-II

NSGA-II was run for 200 generations to obtain Pareto fronts. Figure 10 shows the optimal Pareto fronts obtained by NSGA-II in the multi-objective optimization. It can be seen that optimal solution is a classic shape, convex shape. A Pareto set can provide a designer with 79 design solutions to aid decision making in the design stage.

4.3.3 Results of GRA

Figure 11 shows the grey relational grade results obtained for each solution. Since these grades represent the correlation between the reference and comparable sequences, a large grade implies that the comparability sequence is closely correlated with the reference sequence. In this work, Solution 7 shows the best multi-response characteristics among the 79 solutions considered.

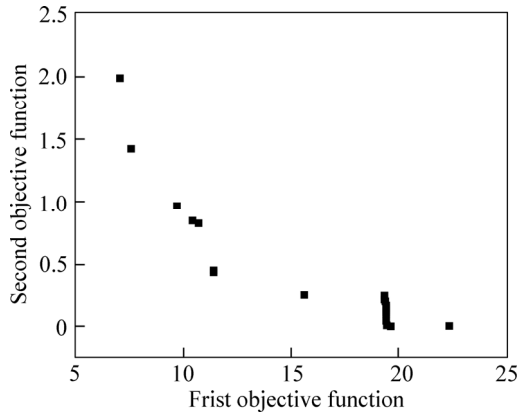

Fig. 10 Optimal Pareto fronts obtained by NSGA-II in multi-objective optimization

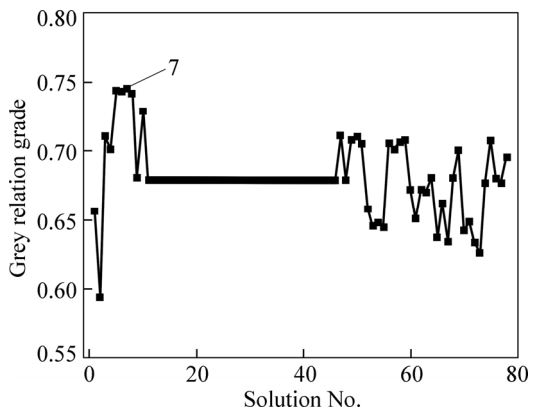

Fig. 11 Grey relational grade results for each solution

4.3.4 Comparison with initial design

A comparison between the parameters obtained by optimization and the initial design parameters is made (see Table 5), and the crimping qualities in both cases from simulation are also compared (Table 6). First, the geometry of the sheet after crimping using the initial design parameters is measured experimentally. Then, the crimping parameters are redesigned according to the optimal solution.

Table 5 Comparison between parameters obtained by optimization and initial design parameters

Parameter	Initial design	Optimal solution
B/mm	190	207.78
R_p/mm	303.2	329.97
β_p/(°)	88	81.29
F_y/kN	3834.05	3243.4

Table 6 Comparison between crimping quality obtained using optimal solution and that using initial design

Parameter indicating crimping quality	Initial design	Optimal solution
L_Z/mm	27.06	23.1
R'/mm	479.38	573.89

As can be seen in Table 5, the forming force is reduced drastically, by 590.65 kN, using the optimal solution. Further, Table 6 indicates that the length of the straight edge is reduced by 3.96 mm and the equivalent radius of curvature is close to nominal radius of curvature of 598.5 mm. From these, it is clear that the crimping quality using the optimal solution is more satisfactory than that using the initial design.

5 Conclusions

1) The optimal solution obtained using the multi-objective optimization approach for crimping is found to give more satisfactory crimping quality than that obtained using the initial design. Thus, the proposed optimization approach is confirmed to be effective for determining an optimal solution of the design of crimping parameters.

2) A set of feasible (i.e. optimal) crimping parameters are obtained through optimization of crimping of a large-diameter longitudinal submerged arc

welded pipe of dimensions *d*1219 mm×22 mm× 12000 mm: the crimp length of 207.78 mm, the base radius of the punch of 329.97 mm, the terminal angle of the punch of 81.29°, and the forming force of 3243.4 kN.

References

[1] LI Hong. Prebending process of longitudinal submerged arc welding production line [J]. Welded Pipe Tube, 2006, 29(1): 55−57. (in Chinese)

[2] XIE Zhi-ming, XIA Jing-ming. Pre-bending process parameter design of longitudinal submerged arc welding pipe [J]. Welded Pipe Tube, 2007, 30(3): 52−54. (in Chinese)

[3] ZHAO Shi-yan. Study on quality control strategy and simulation system development of UOE pipe forming [D]. Qinhuangdao, China: Yanshan University, 2010. (in Chinese)

[4] YANG Qiang. Springback analytic and process parameters optimization of plate edge preflex for the forming of large diameter longitudinal seam welded pipe [D]. Qinhuangdao, China: Yanshan University, 2012. (in Chinese)

[5] FAN Li-feng, GAO Ying, LI Qiang, XU Hong-shen. Quality control on crimping of large diameter welding pipe [J]. Chinese Journal of Mechanical Engineering, 2012, 25(6): 1264−1273.

[6] PALUMBO G, TRICARICO L. Effect of forming and calibration operations on the final shape of large diameter welded tubes [J]. Journal of Materials Processing Technology, 2005, 164−165(5): 1089−1098.

[7] LIU Jin-lei, HUANG Ke-jian, RUAN Feng. Effects of the parameters of prebending on O-forming of pipe in UOE process [J]. Journal of Plasticity Engineering, 2005, 12(3): 72−75. (in Chinese)

[8] HERYNK M D, KYRIAKIDES S, ONOUFRIOU A, YUN H D. Effects of the UOE/UOC pipe manufacturing processes on pipe collapse pressure [J]. International Journal of Mechanical Sciences, 49(5): 533−553.

[9] TONG Xiao-gang. Study on groove shape and the open angle of end tab of UOE pipe [D]. Qinhuangdao, China: Yanshan University, 2008. (in Chinese)

[10] GAO Ying, LI Qiang, FAN Li-feng. Finite element analysis of JCO forming process for longitudinal seam submerged arc welded pipes [J]. Journal of Modelling, Identification and Control, 2010, 11(3/4): 239−249.

[11] REN Qiang, LI Da-yong, ZHOU Tian-xia, PENG Ying-hong. The simulation of UOE pipe forming by three-dimensional finite element method [J]. Journal of Netshape Forming Engineering, 2011, 3(6): 80−84. (in Chinese)

[12] OHATA T, NAKAMURA Y, KATAYAMA T, NAKAMACHI E, NAKANO K. Development of optimum process design system by numerical simulation [J]. Journal of Materials Processing Technology, 1996, 60(1/2/3/4): 543−548.

[13] NACEUR H, GUO Y Q, BATOZ J L, KNOPF-LENOIR C. Optimization of drawbead restraining forces and drawbead design in sheet metal forming process [J]. International Journal of Mechanical Sciences, 2001, 43(10): 2407−2434.

[14] AZAOUZI M, NACEUR H, DELAMEZIERE A, BATOZ J L, BELOUETTAR S. An heuristic optimization algorithm for the blank shape design of high precision metallic parts obtained by a particular stamping process [J]. Finite Elements in Analysis & Design, 2008, 44(14): 842−850.

[15] GUO Y Q, BATOZ J L, NACEUR H, BOUABDALLAH S, ERCIER F, BARLET O. Recent developments on the analysis and optimum design of sheet metal forming parts using a simplified inverse approach [J]. Computers and Structures, 2000, 78: 138−148.

[16] YUSOFF Y, NGADIMAN M S, ZAIN A M. Overview of NSGA-II for optimizing machining process parameters [J]. Procedia Engineering, 2011, 15: 3978−3983.

[17] YANG Yan-zi. Optimization of technologic parameters of mechanical expanding based on neuro network and robust design [D]. Qinhuangdao, China: Yanshan University, 2011. (in Chinese)

[18] XIE Yan-min, YU Hu-ping, CHEN Jun, RUAN Xue-yu. Application of the grey theory in stamping robust design [J]. Journal of Shanghai JiaoTong University, 2007, 41(4): 596−599.

[19] NEVZAT A, ALIREZA A S, HADI A. Multi-objective optimization of some process parameters of a lab-scale thickener using grey relational analysis [J]. Separation and Purification Technology, 2012, 90: 189−195.

[20] CHEN Yi-bao, YAO Jian-chu, ZHONG Yi-fang. A grey difference based multi-objective optimization strategy [J]. Chinese Journal of Mechanical Engineering, 2003, 39(1): 101−106. (in Chinese)

(Edited by YANG Bing)